Volume 51 | Number 51 | 28 June 2015 | Pages 10251–10358

ChemComm

Chemical Communications

www.rsc.org/chemcomm

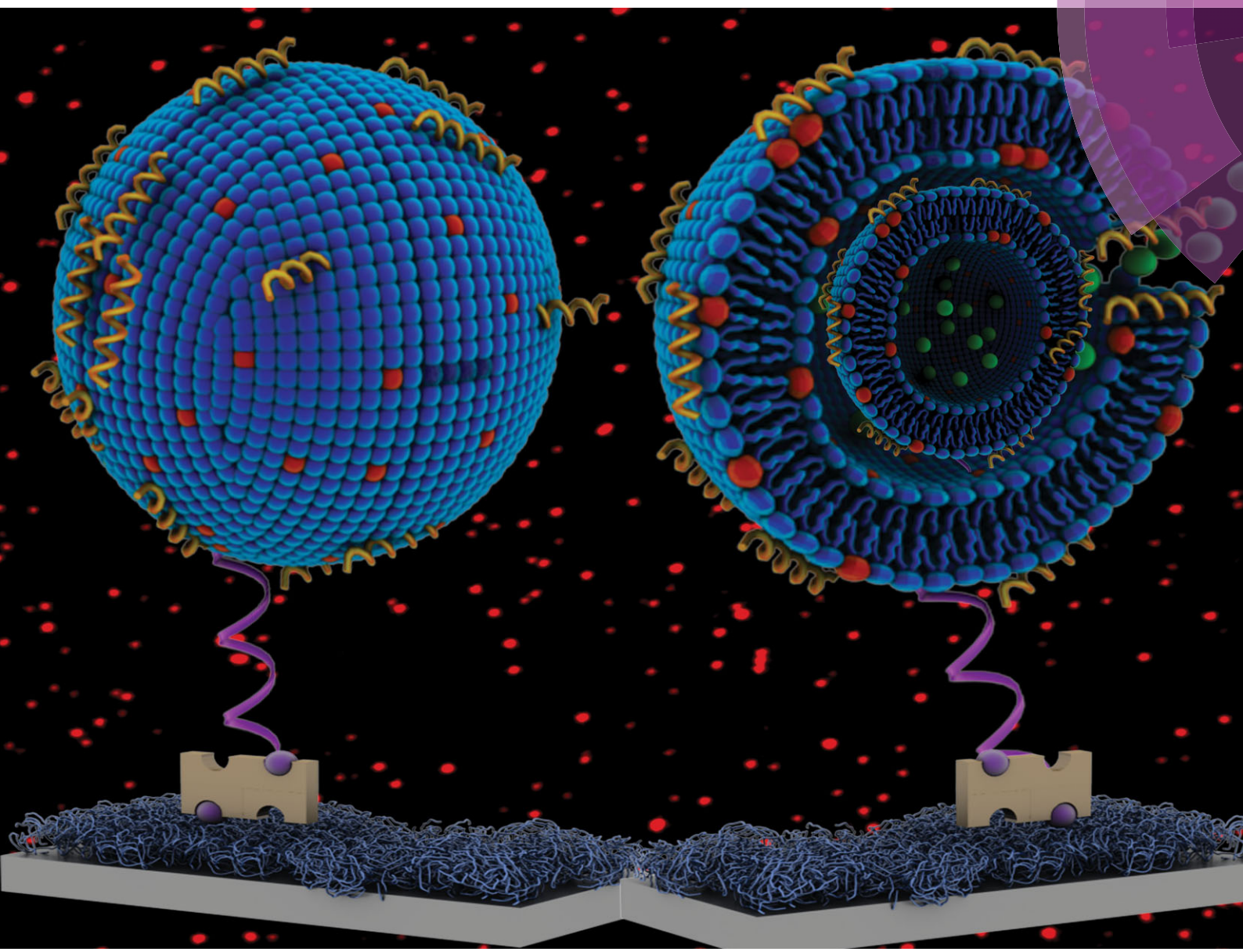

ISSN 1359-7345

ROYAL SOCIETY OF CHEMISTRY

COMMUNICATION

Seyed R. Tabaei and N. J. Cho

Lamellar sheet exfoliation of single lipid vesicles by a membrane-active peptide

ChemComm

COMMUNICATION

View Article Online
View Journal | View Issue

Cite this: *Chem. Commun.*, 2015, 51, 10272

Received 2nd April 2015,
Accepted 6th May 2015

DOI: 10.1039/c5cc02769a

www.rsc.org/chemcomm

Lamellar sheet exfoliation of single lipid vesicles by a membrane-active peptide†

Seyed R. Tabaei[ab] and N. J. Cho*[abc]

Using total internal fluorescence microscopy, highly parallel measurements of single lipid vesicles unexpectedly reveal that a small fraction of vesicles rupture in multiple discrete steps when destabilized by a membrane-active peptide which is in contrast to classical solubilization models. To account for this surprizing kinetic behaviour, we identified that this vesicle subpopulation consists of multilamellar vesicles, and that the outermost lamella is more susceptible to rupture than unilamellar vesicles of even smaller size. This finding sheds light on the multiple ways in which membrane configuration can influence strain in the bilayer leaflet and contribute to nm-scale membrane curvature sensing.

Lipid vesicles are self-closed spherical structures comprised of one or more lipid bilayers surrounding an aqueous cavity.[1] Vesicles with well-defined lipid composition are commonly used as a simple model of biological membranes due to their basic structural resemblance to biomembranes.[2] They can be functionalized by reconstitution of naturally occurring components such as membrane proteins[3] or other functional moieties.[4] This simple biomimetic platform has been used successfully for a range of biological studies including screening of ligand binding to membranes and membrane receptors,[5] protein lipid interactions[6] as well as fundamental studies of membrane fusion[7] and transport.[8] From an analytical perspective, structural properties of vesicles and their associated biological processes can be studied while they are freely diffusing in a suspension or they are immobilized by being tethered to a solid support. Immobilization of vesicles makes them amenable for characterization by using sensitive surface-based analytical techniques such surface plasmon resonance (SPR),[9] quartz crystal microbalance with dissipation (QCM-D)[10] and total internal reflection fluorescence (TIRF) microscopy.[11] In particular, single object fluorescence measurement can be used to resolve multiple individual vesicles tethered on surface if separated by a distance larger than the diffraction limit of light, allowing us to simultaneously investigate several thousand single vesicles.[12] Single vesicle fluorescence measurement can reveal heterogeneities with respect to membrane-associated processes as well as mechanistic and kinetic details, which are hidden in average signals and are not accessible using ensemble measurements. Based on the single-tethered vesicle platform, various mechanistic details of interactions can be followed, including ligand binding,[13] confined reactions,[14] membrane permeability,[15] and membrane fusion.[16] One very important feature of single vesicle imaging is the possibility offered to map the size distribution of vesicles,[17] which enables us to study the dependence of lipid-associated processes on vesicle size, *i.e.*, membrane curvature. By this analysis, detailed information regarding membrane-curvature dependent biological process has been revealed including studies on peptide-membrane interaction,[18] enzyme activity,[19] the size dependence of membrane tension,[20] encapsulation[21] and membrane-protein incorporation efficiency.[15]

We have recently developed a TIRF-based single vesicle assay to investigate membrane-disrupting action of an antiviral α-helical amphipathic (AH) peptide.[18,22] AH peptide is a membrane-active peptide which has been shown to rupture the lipid envelope of lipid vesicles[23] and virus particles[24] such as hepatitis C virus, and serves as a promising template for design of broad spectrum antiviral agents.[25] Our single vesicle fluorescence assay allows us simultaneous monitoring of the onset of membrane poration and rupture of individual vesicles which mimic the lipid membrane of enveloped-viruses, mediated by the action of AH peptide. Briefly, biotinylated lipid vesicles loaded with a water-soluble dye (calcein) and labelled with membrane-residing rhodamine-tagged phospholipid were immobilized on a neutravidin-functionalized glass surface and imaged using TIRF microscopy (Fig. 1a). Upon injection of AH peptide, initially, a slow reduction is observed in the intensity of fluorescence emitted from both calcein and rhodamine dye which was followed by a sharp drop in both intensities (Fig. 1b).

[a] *School of Materials Science and Engineering, Nanyang Technological University, 50 Nanyang Avenue 639798, Singapore. E-mail: njcho@ntu.edu.sg*
[b] *Centre for Biomimetic Sensor Science, Nanyang Technological University, 50 Nanyang Drive 637553, Singapore*
[c] *School of Chemical and Biomedical Engineering, Nanyang Technological University, 62 Nanyang Drive 637459, Singapore*

† Electronic supplementary information (ESI) available: The experimental details and data analysis are included. See DOI: 10.1039/c5cc02769a

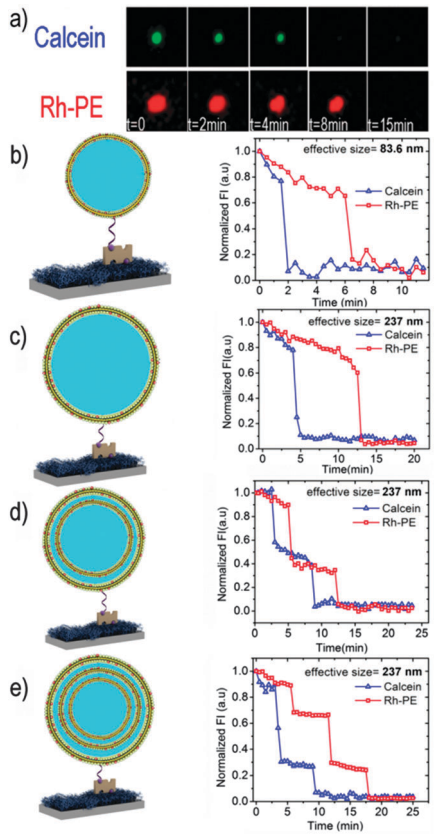

Fig. 1 Simultaneous monitoring of membrane poration and solubilization of individual tethered vesicles mediated by AH peptide. (a) Representative TIRF images obtained through the calcein and rhodamine channels of a single POPC (palmitoyl-2-oleoyl-*sn-glycero*-3-phosphocholine) vesicle (diameter of ~ 237 nm) labeled with rhodamine–POPE (1 wt%) and loaded with calcein, upon interaction with 100 nM AH peptide. Single-step drop in the time traces of the fluorescence intensity of (b) a small (~83 nm) and (c) a large vesicle (~237 nm) upon injection of with 100 nM AH peptide. Representative fluorescence time traces of large vesicles (~237 nm) with (d) double and (e) triple-step fluorescence drop kinetics upon incubation with 100 nM AH peptide. The schematic illustration of tethered vesicles of small unilamellar, large unilamellar and large multilamellar vesicles are also depicted. Biotinylated vesicles were immobilized *via* neutravidin/biotin coupling on a PLL-*g*-PEG/biotin-PEG coated glass surface.

The sharp drop in the intensity of calcein always preceded the similar intensity drop of rhodamine signal. The sudden drop in the calcein signal corresponds to the release of the dye from the vesicle cavity upon vesicle poration. On the other hand, the rhodamine signal drop indicates lipid loss from the TIRF evanescent field caused by peptide-induced membrane solubilization. Fig. 1b and c show the temporal changes observed in two emission channels for a representative single 1-palmitoyl-2-oleoyl-*sn-glycero*-3-phosphocholine (POPC) vesicle with mean diameter of ~80 nm and ~237 nm prepared by extrusion through 50 and 200 nm polycarbonate filters, respectively. Since the action of AH peptide is curvature-dependent, the onset of membrane poration as well as membrane solubilization are shorter in the case of small vesicles (Rh-PE; 6.7 min *vs.* 13 min and calcein; 2 min *vs.* 4.8 min) (Fig. 1b and c). While the fluorescence intensity of the majority of vesicle population exhibit a one-step fluorescence loss due to presumably rupture of vesicle (single step drop from the baseline to the background level), we observed a sub-population of vesicles, which exhibit double (Fig. 1d) and multi-step fluorescence drop kinetics (Fig. 1e). We hypothesized that exhibition of more than one step in the vesicle content release and rupture suggests the presence of more than one layer of membrane in these vesicles, and thus, this multiple drop of fluorescence intensity may reflect the behaviour of multilamellar structures within the vesicle population, which inherently assembled during the extrusion process.[26] Indeed such multi-step fluorescence drop was observed mostly among larger vesicles prepared by extrusion through 200 nm filter. It is known that a fraction of vesicles prepared by extrusion are multilamellar.[27] In particular when the pore size of filter used in extrusion is bigger than 100 nm, the efficiency of breakage of multilamellar vesicles into unilamellar vesicles are reduced and a fraction of vesicles remains with more than one layer of membrane. Therefore the multi-step fluorescence drop kinetics belongs to a population of vesicles with more than one bilayer shells *i.e.*, multilamellar vesicles.

Strikingly, the time scales of the first drop in both signals for vesicles exhibiting multi-step kinetics (Fig. 1d and e) are shorter than the time variation of vesicles that exhibit single step kinetics with the similar size vesicles (Fig. 1c). Fig. 2a and b show the histograms of the onset times of the sharp intensity drop observed in the calcein and rhodamine channels of more than 500 individual large vesicles (mean size ~ 237 nm). Both histogram plots show two maxima (3 and 13 min for rhodamine and 2.1 and 6.1 min for calcein) indicating presence of two populations of vesicles.

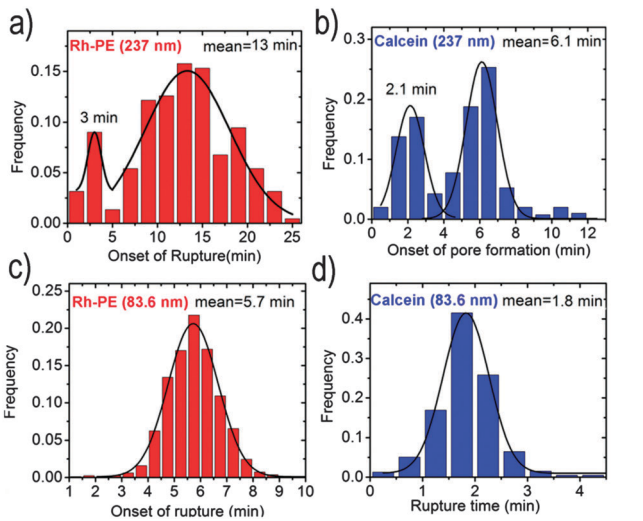

Fig. 2 Statistics of membrane solubilization (rhodamine intensity drop) and content release (calcein intensity drop) of individual vesicles. Histograms of the onset of membrane solubilization (a) and onset of content release (b) of vesicles with mean diameter of 237 nm challenged with 100 nM AH peptide shows two distinct populations. Histograms of the membrane solubilization (c) and content release (d) of small vesicles with mean diameter of 83.6 nm treated with 100 nM AH peptide shows only one maxima at 5.7 and 1.8 min respectively. To create histograms the kinetics traces of more than 500 individual vesicles were analysed. The experiments were repeated three times and representative histograms are displayed.

We further identified and analysed the time traces of fluorescence intensity with shorter time scales (vesicles with Rh-PE signal drop of <5 min). The analysis revealed that indeed the fluorescence traces belonging to the populations with shorter time scale exhibit multi-step kinetics, corresponding to characteristics of multilamellar vesicles. However, almost all vesicles belonging to the population with longer time scale (13 and 6.1 min for rhodamine and calcein, respectively) exhibit single step kinetic. As expected, in marked contrast to large vesicles, single distribution was observed in the histograms of calcein and rhodamine release from small vesicles (mean size $\sim$ 83 nm) (Fig. 2c and d). Previously we have shown that AH peptide is curvature sensitive,[18] thus it is expected that the onset of membrane poration and rupture of small vesicles to be shorter than those of large vesicles. The observation support that the first layer of large multilamellar vesicles treated by AH peptide destabilized faster than unilamellar vesicles of smaller size, suggesting multilamellarity may affect the membrane stability.

The aforementioned interpretation which suggests that multi-step fluorescence drop kinetics belongs to vesicles having more than one bilayer shell, gains additional support from studying the size distribution of small and large vesicle populations. The size of individual vesicles can be determined from the intensity of the fluorescence emitted from membrane residing rhodamine dye, as the concentration of the dye in the membrane, and hence its corresponding fluorescence intensity is proportional to the vesicle surface area. Therefore the vesicle radius is proportional to the square root of the vesicle's rhodamine signal. The histogram plot for the square root of the rhodamine signal of large vesicles depicts two peaks with mean value of $\text{mean}_{\text{large1}} = 90$ and $\text{mean}_{\text{large2}} = 174$ (Fig. 3a). However the size distribution of these vesicles obtained by dynamic light scattering (DLS) only shows one maxima at 237 nm. Interestingly the ratio of the two maxima in the rhodamine intensity histogram is $\sim$0.5 ($\text{mean}_{\text{large1}}/\text{mean}_{\text{large2}}$), suggesting that the surface area of vesicles with higher intensity value ($\text{mean}_{\text{large2}} = 174$) is twice those of vesicles with lower mean intensity ($\text{mean}_{\text{large1}} = 90$). However, since the DLS distribution does not show two discrete peaks, the only explanation would be that vesicles with higher intensity consist of two bilayers. In addition, analysis of the fluorescence traces of the vesicle fraction with higher intensity revealed exhibition of multi-step kinetics, further supporting that multilamellar vesicles exhibit multi-step kinetics. In contrast to large vesicles, the histogram plot for the square root of the rhodamine signal of small vesicles only depicts one maxima ($\text{mean}_{\text{small}} = 39.3$) similar to its corresponding size distribution obtained by DLS (Fig. 3b). Further single vesicle analysis allowed quantification of fraction of vesicles with single, double and triple step kinetics in each batch of vesicles (Fig. 3c). The majority ($>$95%) of small vesicles with mean diameter of $\sim$83 nm was found to exhibit single step kinetics while less than 5% of these vesicles showed double step kinetics and no vesicles were found which showed triple step kinetics. Nearly 85% of large vesicles with mean diameter of $\sim$237 nm showed single step kinetics. Almost 10% of large vesicles exhibit double step kinetics. The share of large vesicles with triple step kinetics was about 5%. These findings are in agreement with previous reports on the multilamellar fraction of the 100 and 200 nm vesicles prepared by extrusion.[28]

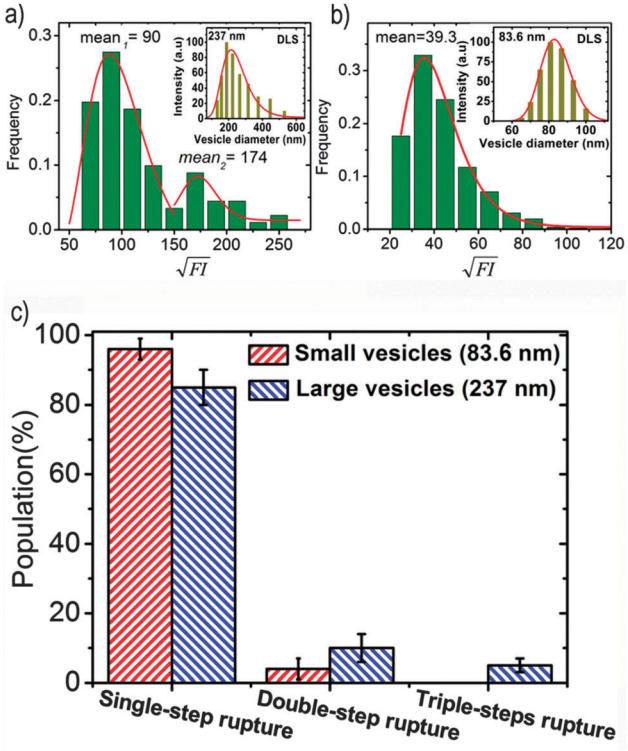

Fig. 3 Size distribution of vesicles obtained by fluorescence intensity of membrane-residing rhodamine dye and DLS. (a) Distribution of square root of fluorescence intensity of more than 500 individual vesicles prepared by extrusion through 200 nm polycarbonate filter shows two discrete maxima. The inset shows the size distribution of vesicles obtained by DLS (mean diameter: 237 nm). (b) Histogram plot of square root of fluorescence intensity of vesicles prepared by extrusion through 50 nm polycarbonate filter. The inset depicts the size distribution of vesicles obtained by DLS (mean diameter: 83.6 nm). (c) Summary of fraction of vesicles exhibiting single, double and triple step kinetics in small ($\sim$83.6 nm) and large vesicles (237 nm).

In summary, a TIRF-based single tethered vesicle assay was used to study the interaction of an α-helical amphipathic peptide with lipid vesicles. Simultaneous monitoring of membrane poration and rupture of individual tethered vesicles mediated by AH peptide revealed that a fraction of vesicles (15%) prepared by extrusion through 200 nm filter, exhibit more than one step in the poration and rupture suggesting the presence of more than one layer of membrane in these vesicles. The multistep release profile of MLVs can be used as design guidelines for development of drug delivery vehicles for intermittent drug release applications based on active degradation of membrane specifically in the tumor tissue.[29] The outermost lamella of multilamellar vesicles was found to be more susceptible to poration and rupture in comparison to a unilamellar vesicle with even smaller size. The structure of MLVs resemble the membrane organization of intracellular organelles such as multilamellar bodies (MLBs)[30] as well as multilaminar lysosomes[31] which are composed of concentric membrane layers. Such structures are highly dynamics and undergo major structural changes during chemical loading and release. The susceptibility of the outermost

lamella of MLVs, might provide a physical drive in the physicochemical mechanism that govern the stability and dynamics of such organelles. This finding sheds light on the multiple ways in which vesicle structure can influence the interaction between a membrane-active peptide and lipid vesicles. The results also suggest the potential of our TIRF-based assay for structural characterization of individual vesicles.

This work was supported by the National Research Foundation (NRF-NRFF2011-01) and the National Medical Research Council (NMRC/CBRG/0005/2012).

Notes and references

1 D. D. Lasic, *Biochem. J.*, 1988, **256**, 1.
2 G. Sessa and G. Weissmann, *J. Lipid Res.*, 1968, **9**, 310.
3 J.-L. Rigaud, B. Pitard and D. Levy, *Biochim. Biophys. Acta, Bioenerg.*, 1995, **1231**, 223.
4 J. Connor, S. Sullivan and L. Huang, *Pharmacol. Ther.*, 1985, **28**, 341.
5 M. A. Cooper, *J. Mol. Recognit.*, 2004, **17**, 286.
6 H. Zhu, M. Bilgin, R. Bangham, D. Hall, A. Casamayor, P. Bertone, N. Lan, R. Jansen, S. Bidlingmaier and T. Houfek, *Science*, 2001, **293**, 2101.
7 J. Wilschut and D. Hoekstra, *Trends Biochem. Sci.*, 1984, **9**, 479.
8 M. Brändén, S. R. Tabaei, G. Fischer, R. Neutze and F. Höök, *Biophys. J.*, 2010, **99**, 124.
9 J. Homola, *Chem. Rev.*, 2008, **108**, 462.
10 N.-J. Cho, C. W. Frank, B. Kasemo and F. Höök, *Nat. Protoc.*, 2010, **5**, 1096.
11 H. Schneckenburger, *Curr. Opin. Biotechnol.*, 2005, **16**, 13.
12 S. M. Christensen and D. Stamou, *Soft Matter*, 2007, **3**, 828.
13 N. S. Hatzakis, V. K. Bhatia, J. Larsen, K. L. Madsen, P.-Y. Bolinger, A. H. Kunding, J. Castillo, U. Gether, P. Hedegård and D. Stamou, *Nat. Chem. Biol.*, 2009, **5**, 835.
14 H. Pick, E. L. Schmid, A.-P. Tairi, E. Ilegems, R. Hovius and H. Vogel, *J. Am. Chem. Soc.*, 2005, **127**, 2908.
15 G. Ohlsson, S. R. Tabaei, J. Beech, J. Kvassman, U. Johanson, P. Kjellbom, J. O. Tegenfeldt and F. Höök, *Lab Chip*, 2012, **12**, 4635.
16 T.-Y. Yoon, B. Okumus, F. Zhang, Y.-K. Shin and T. Ha, *Proc. Natl. Acad. Sci. U. S. A.*, 2006, **103**, 19731.
17 A. H. Kunding, M. W. Mortensen, S. M. Christensen and D. Stamou, *Biophys. J.*, 2008, **95**, 1176.
18 S. R. Tabaei, M. Rabe, V. P. Zhdanov, N.-J. Cho and F. Höök, *Nano Lett.*, 2012, **12**, 5719.
19 M. Rabe, S. R. Tabaei, H. Zetterberg, V. P. Zhdanov and F. Höök, *Angew. Chem., Int. Ed.*, 2015, **54**, 1022.
20 P. M. Bendix, M. S. Pedersen and D. Stamou, *Proc. Natl. Acad. Sci. U. S. A.*, 2009, **106**, 12341.
21 B. Lohse, P.-Y. Bolinger and D. Stamou, *J. Am. Chem. Soc.*, 2008, **130**, 14372.
22 J. A. Jackman, R. Saravanan, Y. Zhang, S. R. Tabaei and N. J. Cho, *Small*, 2015, DOI: 10.1002/smll.201403638.
23 (*a*) N.-J. Cho, S.-J. Cho, K. H. Cheong, J. S. Glenn and C. W. Frank, *J. Am. Chem. Soc.*, 2007, **129**, 10050; (*b*) J. A. Jackman, H. Z. Goh, V. P. Zhdanov and N.-J. Cho, *J. Phys. Chem. B*, 2013, **117**, 16117; (*c*) H. Z. Goh, J. A. Jackman and N.-J. Cho, *J. Phys. Chem. B*, 2014, **118**, 3616; (*d*) H. Z. Goh, J. A. Jackman, S.-O. Kim and N.-J. Cho, *Small*, 2014, **10**, 4828.
24 N.-J. Cho, H. Dvory-Sobol, A. Xiong, S.-J. Cho, C. W. Frank and J. S. Glenn, *ACS Chem. Biol.*, 2009, **4**, 1061.
25 J. A. Jackman and N.-J. Cho, *Biointerphases*, 2012, **7**, 18.
26 J. A. Jackman, Z. Zhao, V. P. Zhdanov, C. W. Frank and N.-J. Cho, *Langmuir*, 2014, **30**, 2152.
27 L. Mayer, M. Hope and P. Cullis, *Biochim. Biophys. Acta, Biomembr.*, 1986, **858**, 161.
28 (*a*) C. Lohr, A. H. Kunding, V. K. Bhatia and D. Stamou, *Methods Enzymol.*, 2009, **465**, 143; (*b*) E. C. Heider, M. Barhoum, K. Edwards, K.-H. Gericke and J. M. Harris, *Anal. Chem.*, 2011, **83**, 4909.
29 T. L. Andresen, S. S. Jensen and K. Jørgensen, *Prog. Lipid Res.*, 2005, **44**, 68.
30 G. Schmitz and G. Müller, *J. Lipid Res.*, 1991, **32**, 1539.
31 J. L. A. Murk, M. N. Lebbink, B. M. Humbel, W. J. Geerts, J. M. Griffith, D. M. Langenberg, F. A. Verreck, A. J. Verkleij, A. J. Koster and H. J. Geuze, *Traffic*, 2004, **5**, 936.